Inorganic Chemistry
Article

Inorg. Chem. **2009**, *48*, 11767–11778 **11767**
DOI: 10.1021/ic901779k

Solid State and Solution Dynamics of Pyridine Based Tetraaza-Macrocyclic Lanthanide Chelates Possessing Phosphonate Ligating Functionality (Ln-PCTMB): Effect on Relaxometry and Optical Properties

Garry E. Kiefer*,† and Mark Woods‡,§

†*Macrocyclics, 2110 Research Row, Dallas, Texas 75235,* ‡*Department of Chemistry, Portland State University, P.O. Box 751, Portland, Oregon 97207, and* §*Advanced Imaging Research Center, Oregon Health and Sciences University, 3181 S.W. Sam Jackson Park Road, L452, Portland, Oregon 97239*

Received September 5, 2009

The macrocyclic ligand 3,6,9-tris(methylenebutyl phosphonic acid)-3,6,9−15-tetraazabicyclo [9.3.1]pentadeca-1(15),11,13-triene (PCTMB) was synthesized and complexes of Eu^{3+}, Tb^{3+}, and Gd^{3+} studied by X-ray crystallography, luminescence, and relaxometry. In the crystal these complexes are dimeric and possess 8-coordinate Ln^{3+} centers that are linked by bridging phosphonates. The rigidity introduced by the pyridyl nucleus forces the EuPCTMB and TbPCTMB to adopt a twisted snub disphenoid (TSD) coordination geometry. Examination of the $^5D_0 \rightarrow {}^7F_0$ luminescent transition of EuPCTMB in the solid state confirmed the existence of a single distinct Eu^{3+} coordination environment, whereas two Eu^{3+} coordination environments were observed in aqueous solution. Lifetime analysis of aqueous TbPCTMB solutions determined that $q = 0.1$ and $q = 1.0$ for the two coordination environments and Stern−Volmer quenching constants ($K_{SV}^{\tau} = 1101\ M^{-1}$, $K_{SV}^{\Phi} = 40780\ M^{-1}$) support the presence of a complicated monomer/dimer equilibrium. Relaxivity studies of GdPCTMB in H_2O/CH_3OH exhibited a concentration dependency (0.02 mM−10.00 mM) ranging from $r_1 = 7.0\ mM^{-1}\ s^{-1}$ to $4.0\ mM^{-1}\ s^{-1}$ consistent with the trend observed by luminescence.

Introduction

The lanthanide series of metal ions possess a diverse array of physical properties that have been the source of many technological innovations over the years.[1] In particular, lanthanides have become invaluable components for contrast enhancement media used in nuclear medicine, for magnetic resonance imaging, and as optical probes. Equally important for advancing their use in medicine has been the molecular architecture of tailored ligand systems that can provide an optimal coordination environment for maximum stability; a requirement for rendering the metal ion inert and non-toxic for in vivo applications. Furthermore, the organic ligand framework can function to enhance photophysical properties[2−5] and modulation of water exchange kinetics in the chelate structure.[6−8] For biological applications, the cumulative body of knowledge has clearly demonstrated that the high thermodynamic and kinetic inertness of chelates formed between Ln^{3+} ions and polyaza-macrocyclic ligand systems is a paramount feature for safeguarding long-term chelate integrity.[9] Of considerable interest in this regard is the family of chelates derived from 1,4,7,10-tetraazacyclododecane (cyclen) which is a familiar signature of many Magnetic Resonance Imaging (MRI) and radiopharmaceutical contrast agents in clinical use and under development.

The versatility of cyclen-based ligands for lanthanide coordination is evidenced by the many related analogues present in the literature that are designed for enhancing various aspects of performance through structural "fine tuning". A noteworthy example reported over 25 years ago is the 12-membered tetraaza-macrocyclic ligand which incorporates a pyridine nucleus within the macrocyclic ring, pyclen.[10]

*To whom correspondence should be addressed. E-mail: garry@macrocyclics.com. Phone: + 1 972 250 2248. Fax: + 1 972 250 2245.

(1) Bunzli, J. C. G.; Choppin, G. R. *Lanthanide Probes in Life, Chemical and Earth Sciences: Theory and Practice*; Elsevier: Amsterdam, 1990.
(2) Parker, D.; Williams, J. A. G. *J. Chem. Soc., Dalton Trans.* **1996**, *18*, 3613–3628.
(3) Parker, D. *Coord. Chem. Rev.* **2000**, *205*, 109–130.
(4) Parker, D.; Dickins, R. S.; Puschmann, H.; Crossland, C.; Howard, J. A. K. *Chem. Rev.* **2002**, *102*(6), 1977–2010.
(5) Faulkner, S.; Pope, S. J. A.; Burton-Pye, B. P. *Appl. Spectrosc. Rev.* **2005**, *40*(1), 1–31.
(6) Sherry, A. D.; Zhang, S.; Woods, M. Water Exchange is the Key Parameter in the Design of Next Generation MRI Agents. In *Medicinal Inorganic Chemistry*; Sessler, J. L., Doctrow, S. R., McMurray, T. J., Lippard, S. J., Eds.; ACS Symposium Series 903; American Chemical Society: Washington, D.C., 2005; pp 151−165.
(7) Woods, M.; Sherry, A. D., Engineering Lanthanide Complexes with Controlled Water Exchange Rates for Magnetic Resonance Imaging. *Proceedings of the 26th Ann. Intl. Conf. IEEE EMBS*, **2004**, pp 5254−5257.
(8) Woods, M.; Zhang, S.; Sherry, A. D. *Curr. Med. Chem.* **2004**, *4*(4), 349–369.
(9) Caravan, P.; Ellison, J. J.; McMurry, T. J.; Lauffer, R. B. *Chem. Rev.* **1999**, *99*(9), 2293–2352.
(10) Stetter, H.; Frank, W.; Mertens, R. *Tetrahedron* **1981**, *37*(4), 767–72.

Published on Web 11/12/2009

The aminocarboxylic acid derivative of pyclen, PCTA, is known to form stable lanthanide chelates (log K_{GdL} = 20.39),[11] its Gd^{3+} chelate was also considered as a neutrally charged, general perfusion MRI contrast agent.[12] Surprisingly, however, these fascinating derivatives have received far less attention than their cyclen-based counterparts. Recently pyclen-based ligands have been rediscovered through several reports that survey the effect of structural morphology upon water exchange kinetics in lanthanide chelates; a potentially useful tool for optimizing the performance of MR contrast media.[13−15] In addition, these same ligands have been found to possess rapid chelation kinetics under very mild conditions thus stimulating renewed interest for nuclear medicine applications where the time required for complexation to occur is an important concern.[11]

Our interest in the pyclen family of chelates (Chart 1) stems from their unique multimodal imaging potential and the ability to control in vivo tissue targeting through alterations of ligating functionality. In particular it has been demonstrated that incorporation of a phosphonate ester ligating functionality provides an efficient means of altering biodistribution properties and for selective targeting of cancer.[16] In the case of highly lipophilic phosphonate chelates the formation of non-covalent dimers has been inferred to be an important aspect of the cellular targeting process. To gain a better understanding of the chemistry responsible for these observations we undertook a study of the solid state and solution behavior of a pyclen-phosphonate chelate which has been suggested to dimerize in aqueous media. Herein is presented a detailed analysis of the solid state crystal data and solution dynamics that are relevant to the design of targeted diagnostic and therapeutic agents structured around the lanthanide chelate.

Chart 1

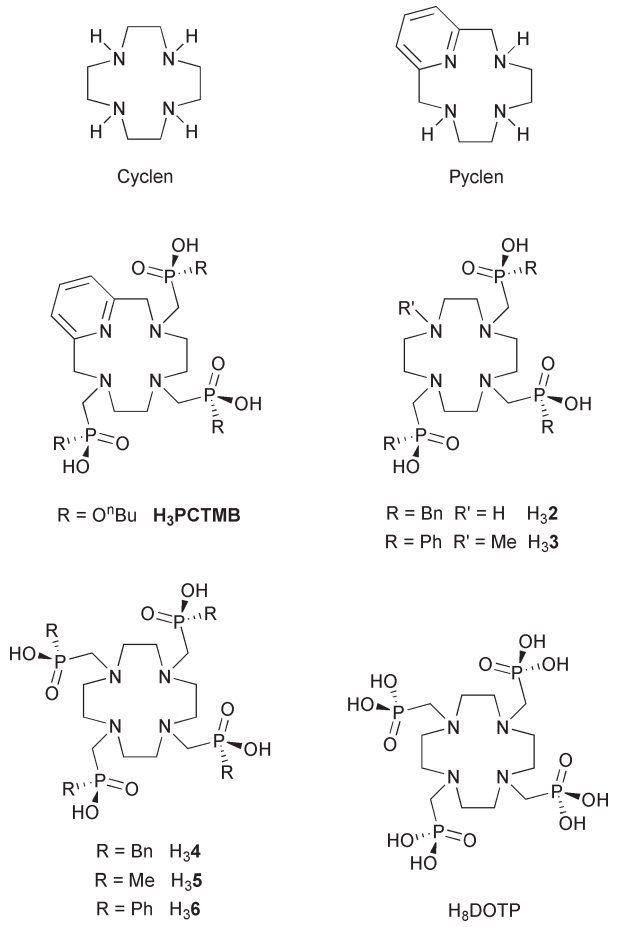

Experimental Section

General Remarks. All solvents and reagents were purchased from commercial sources and used as received unless otherwise stated. ^{1}H, ^{13}C, and ^{31}P NMR spectra were recorded on a Varian Mercury spectrometer operating at 299.99, 75.43, and 121.44 MHz, respectively. Infrared spectra were recorded on a Perkin-Elmer 1600 Series FTIR. 3, 6, 9, 15-tetraazabicyclo[9.3.1] pentadeca-1(15), 11, 13-triene (pyclen) was prepared using previously published methods.[10]

3,6,9-Tris[methylene(dibutylphosphonate)]-3,6,9,15-tetraazabicyclo[9.3.1] pentadeca-1(15), 11, 13-triene (1). Paraformaldehyde (1.2 g, 38.2 mmol) was added to a solution of 3, 6, 9, 15-tetraazabicyclo[9.3.1]pentadeca-1(15), 11, 13-triene (2.5 g, 12.1 mmol) in tetrahydrofuran (THF, 30 mL), and the resulting slurry stirred at ambient temperature for 30 min. Tri-*n*-butyl phosphite (9.6 g, 38.2 mmol) was then added, and the turbid reaction mixture stirred for an additional 72 h at ambient temperature. The resulting homogeneous reaction mixture was concentrated in vacuo to give a pale yellow, viscous oil (10.0 g). The crude product was purified by column chromatography on basic alumina (5 × 26 cm) eluting with chloroform. Two fractions were collected (2 column volumes) beginning with the second column volume of eluent. After concentration in vacuo the product was isolated as colorless oil (9.06 g, 92%). ^{1}H NMR (300 MHz, $CDCl_3$) δ = 0.87 (m, CH_3, 18H), 1.35 (m, CH_2, 12H), 1.59 (m, CH_2, 12H), 2.62 (m, CH_2, 4H), 2.74 (m, CH_2, 10H), 3.05 (d, CH_2, $^2J_{PH}$ 10 Hz, 4H), 4.01 (m, OCH_2, 12H), 7.17 (d, 3-Ar, $^3J_{HH}$ 8 Hz, 2H), 7.58 (t, 4-Ar, $^3J_{HH}$ 8 Hz, 1H); ^{13}C NMR (75 MHz, $CDCl_3$) δ = 13.5 (CH_3), 13.52 (CH_3), 18.6 (CH_2), 18.7 (CH_2), 32.2 (d, CH_2, $^3J_{PC}$ 6 Hz), 32.5 (d, CH_2, $^3J_{PC}$ 6 Hz), 50.1 (d, CH_2, $^2J_{PC}$ 8 Hz), 51.2 (d, CH_2, $^1J_{PC}$ 157 Hz), 51.2 (d, CH_2, $^2J_{PC}$ 10 Hz), 51.9 (d, CH_2, $^1J_{PC}$ 157 Hz), 60.8 (CH_2), 65.6 (d, CH_2, $^3J_{PC}$ 6 Hz), 67.2 (d, $^2J_{PC}$ 6 Hz), 123.0 (3-Ar), 137.0 (2-Ar), 157.2 (4-Ar); ^{31}P[^{1}H] NMR (121.44 MHz, $CDCl_3$) δ = 24.94 (2P), 24.96 (1P). *m*/*z*: (ESI+); 826 (100% $[M + H]^+$.

3,6,9-Tris[methylene(butylphosphonate)]-3,6,9−15-tetraazabicyclo [9.3.1]pentadeca-1(15),11,13-triene potassium salt (K_3P-CTMB). A solution of the hexa-ester **1** (9.06 g, 11.36 mmol) and KOH (7.65 g, 136.3 mmol) in water (100 mL) and 1,4-dioxane (30 mL) was heated to reflux for 18 h. The reaction mixture was then cooled and filtered while warm. The filtrate was concentrated to give a solid which was suspended in 5:1 v/v $CHCl_3$/MeOH (200 mL) and heated to reflux. The hot solution was filtered, and the solvent removed from the filtrate in vacuo to afford an off-white solid. The residue was taken up into $CHCl_3$ (60 mL) with stirring followed by the addition of CH_3CN in small portions until the solution became slightly turbid. Upon

(11) Tircso, G.; Kovacs, Z.; Sherry, A. D. *Inorg. Chem.* **2006**, *45*(23), 9269–9280.
(12) Gries, H.; Raduchel, B.; Platzek, J.; Press, W.; Speck, U. Macrocyclic Polyaza Bicyclo Compounds Containing 5 or 6 Membered Rings, and Methdods for MRI; **1994**.
(13) Aime, S.; Botta, M.; Crich, S. G.; Giovenzana, G.; Pagliarin, R.; Sisti, M.; Terreno, E. *Magn. Reson. Chem.* **1998**, *36*, S200–S208. (Spec. Issue).
(14) Aime, S.; Botta, M.; Frullano, L.; Crich, S. G.; Giovenzana, G.; Pagliarin, R.; Palmisano, G.; Sirtori, F. R.; Sisti, M. *J. Med. Chem.* **2000**, *43* (21), 4017–4024.
(15) Aime, S.; Gianolio, E.; Corpillo, D.; Cavallotti, C.; Palmisano, G.; Sisti, M.; Giovenzana, G. B.; Pagliarin, R. *Helv. Chim. Acta* **2003**, *86*(3), 615–632.
(16) Young, S. A.; Kiefer, G. E.; Depalatis, L. R. Synthesis and cell permeability of targeting aminophosphonic acid-based chelants and chelates and their use for treatment of cancer. *PCT. Int. Appl.* 2006020779 A2 20060223.

cooling with continued stirring in an ice bath a white precipitate was observed. The precipitate was isolated by filtration and washed with CH_3CN. After drying in vacuo, the title compound was isolated as a colorless solid (4.14 g, 49%). mp: 150−160 °C, dec.; ^{1}H NMR (300 MHz, D_2O) δ = 0.78 (m, CH_3, 9H), 1.22 (m, CH_2, 6H), 1.43 (m, CH_2, 6H), 2.47 (m, CH_2, 6H), 2.81 (m, CH_2, 10H), 3.65 (d, CH_2, $^2J_{PH}$ 10 Hz, 4H), 4.84 (m, OCH_2, 6H), 7.22 (d, 3-Ar, $^3J_{HH}$ 8 Hz, 2H), 7.63 (t, 4-Ar, $^3J_{HH}$ 8 Hz, 1H); ^{13}C NMR (75 MHz, D_2O) δ = 15.9 (CH_3), 21.3 (CH_2), 35.2 (CH_2), 35.2 (CH_2), 52.0 (CH_2), 52.9 (CH_2), 55.9 (d, $^1J_{PC}$ 144 Hz), 62.5 (CH_2), 67.2 (d, -OCH_2, $^2J_{PC}$ 6 Hz), 126.3 (3-Ar), 141.7 (2-Ar), 159.7 (4-Ar); ^{31}P[^{1}H] (121.44 MHz, D_2O) δ = 20.59; IR υ_{max}/cm^{-1}: 1211 (P═O), 1068 (P−O−C); *m*/*z*: (ESI+); 695 (100% $[M + H_3 + K]^+$; Anal. Found C 35.4 H 5.9 N 5.7, $C_{26}H_{48}K_3N_4O_9P_3 \cdot 2.5CH_3OH \cdot 2KOH$ requires C. 35.5 H 6.3 N. 5.8.

General Procedure for the Preparations of LnPCTMB Chelates. K_3PCTMB (352 mg, 0.4 mmol) was dissolved in water (5 mL), and the strongly basic solution adjusted to pH 5 via dropwise addition of 6N HCl. An aqueous $LnCl_3$ solution (0.4 mmol in 1.5 mL) was then added to the ligand in 200 μL aliquots. The reaction was stirred throughout, and the pH maintained close to 5 by addition of a 1N KOH solution. Following the addition of each $LnCl_3$ aliquot, chelation progress was monitored by RP- HPLC (Phenomenex PRP-1 C18 column (4.6 × 250 mm), 1 mL/min, 80:20 v/v methanol/water, λ = 266 nm; ligand t_R = 6 min, chelate t_R = 10 min.). When all the free ligand was found to be consumed the aqueous solution was filtered through a 0.2 μm syringe filter and lyophilized to give the chelate as a flocculent white solid. Each chelate was then dissolved in a minimum of boiling water and, upon cooling, was found to crystallize as a colorless solid.

Europium (III) 3,6,9-Tris[methylene(butylphosphonate)]-3,6,9−15-tetraazabicyclo [9.3.1]pentadeca-1(15),11,13-triene (EuPCTMB). *m*/*z*: (ESI+); 807 (100%, $[EuLH]^+$, an appropriate isotope pattern was observed); IR υ_{max}/cm^{-1}: 1234 (P═O), 1054 (P−O−C); Anal. Found: C 34.9, H 6.1, N 6.2, $C_{26}H_{48}N_4O_9$ $KP_3Eu \cdot 3H_2O$ requires C 34.8, H 6.1, N 6.2.

Gadolinium(III) 3,6,9-Tris[methylene(butylphosphonate)]-3,6,9−15-tetraazabicyclo [9.3.1]pentadeca-1(15),11,13-triene (GdPCTMB). *m*/*z*: (ESI+); 812 (100% $[GdLH]^+$, an appropriate isotope pattern was observed); IR υ_{max}/cm^{-1}: 1235 (P═O), 1054 (P−O−C); Anal. Found: C 35.2, H 6.2, N 6.3, $C_{26}H_{48}N_4O_9$ $KP_3Gd \cdot 2H_2O$ requires C 35.3, H 6.0, N 6.3.

Terbium(III) 3,6,9-Tris[methylene(butylphosphonate)]-3,6,9−15-tetraazabicyclo [9.3.1]pentadeca-1(15),11,13-triene (TbPCTMB). *m*/*z*: (ESI+); 813 (100% $[TbLH]^+$, an appropriate isotope pattern was observed); IR υ_{max}/cm^{-1}: 1234 (P═O), 1054 (P−O−C); Anal. Found: C 34.5, H 6.0, N 6.1, $C_{26}H_{48}N_4O_9$ $KP_3Tb \cdot 3H_2O$ requires C 34.5, H 6.0, N 6.2.

X-ray Crystallography Data Collection. $[EuPCTMB]_2 \cdot 9H_2O$ and $[TbPCTMB]_2 \cdot 925H_2O$. A Leica Z microscope was used to identify a suitable colorless needle 0.3 mm × 0.08 mm × 0.03 mm from a representative sample of crystals of the same habit. The crystal was coated in a cryogenic protectant (paratpne), and was then fixed to a loop which in turn was fashioned to a copper mounting pin. The mounted crystal was then placed in a cold nitrogen stream (Oxford) maintained at 110 K.

A Bruker SMART 1000 X-ray three-circle diffractometer was employed for crystal screening, unit cell determination, and data collection. The goniometer was controlled using the Smart software suite (Microsoft operating system). The sample was optically centered with the aid of a video camera such that no translations were observed as the crystal was rotated through all positions. The detector was set at 5.0 cm from the crystal sample (CCD-, 512 × 512 pixel). The X-ray radiation employed was generated from a Mo sealed X-ray tube (K_α = 0.70173 Å with a potential of 50 kV and a current of 40 mA) and filtered with a graphite monochromator in the parallel mode (175 mm collimator with 0.8 mm pinholes).

Dark currents were obtained for the appropriate exposure time of 10 s, and a rotation exposure was taken to determine crystal quality and the X-ray beam intersection with the detector. The beam intersection coordinates were compared to the configured coordinates, and changes were made accordingly. The rotation exposure indicated acceptable crystal quality, and the unit cell determination was undertaken. Forty data frames were taken at widths of 0.3° with an exposure time of 10 s. Over 200 reflections were centered, and their positions were determined. These reflections were used in the autoindexing procedure to determine the unit cell. A suitable cell was found and refined by non-linear least-squares and Bravais lattice procedures and reported. The unit cell was verified by examination of the *hkl* overlays on several frames of data including zone photographs. No supercell or erroneous reflections were observed.

After careful examination of the unit cell, a standard data collection procedure was initiated. This procedure consists of collection of one hemisphere of data collected using ω scans, involving the collection over 2400 0.3° frames at fixed angles for ϕ, 2θ, and χ (2θ = −28°, χ = 54.73°), while varying ω. Each frame was exposed for 20 s and contrasted against a 20 s dark current exposure. The total data collection was performed for duration of approximately 15 h at 110 K. No significant intensity fluctuations of equivalent reflections were observed. After data collection the crystal was measured carefully for size, morphology, and color.

Luminescent Measurements. Steady state and lifetime measurements were performed on an Edinburgh Instruments FL/FS900CDT fluorometer equipped with a 450 W xenon arc lamp and a 100 W μF 920H flash lamp. High resolution emission spectra (ΔJ = 0) were recorded from 578.5 to 582.0 nm using a 0.05 nm emission monochromator step size (λ_{ex} = 270 nm). Full emission spectra were recorded from 525−725 nm using a 0.25 nm step size. For Stern−Volmer static and dynamic quenching constant measurements λ_{ex} = 270 nm, λ_{em} = 616 nm. Solutions of EuPCTMB were prepared at 0.01 mM with varying quencher concentration (NdPCTMB) ranging from 0.0 mM−0.04 mM. All solutions were stirred for 1 h at 60 °C and then equilibrated for 4 h at room temperature prior to measurements.

Results and Discussion

Synthesis. Pyclen was synthesized according to a procedure described by Stetter et al.[10] Subsequently, pyclen was reacted with paraformaldehyde and tributyl phosphite in THF to afford the hexa-butyl phosphonate **1**. Selective hydrolysis of the ester intermediate to the mono ester was achieved under basic hydrolysis conditions using 1 equiv of KOH per phosphonate in dioxane and water. The hydrolysis reaction was followed using ^{31}P NMR by monitoring the disappearance dialkyl phosphonate ester resonances at 25 ppm and the appearance of the monoester resonances at approximately 20 ppm. Upon completion, the reaction mixture was concentrated, and the crude product crystallized as the potassium salt from $CHCl_3/CH_3CN$. Lanthanide chelates were then prepared by acidifying an aqueous solution of K_3PCTMB (pH 5) followed by aqueous $LnCl_3$ in small aliquots. The pH was maintained between 5 and 6 by addition of small amounts of a KOH solution, and the chelation reaction was monitored by RP-HPLC (Scheme 1). When all the free ligand was consumed the aqueous solution was freeze-dried and crystallized from hot water to afford X-ray quality crystals.

Scheme 1. Preparation of PCTMB from Pyclen[a]

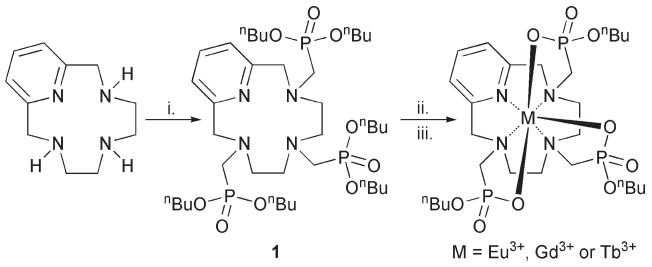

[a] Reagents and conditions: (i) $(CH_2O)_n/(^nBuO)_3P/THF$; (ii) KOH/1,4-dioxane/H_2O; (iii) $LnCl_3/H_2O$/pH 5.5.

Crystallographic Studies. X-ray diffraction of single crystals of Eu**1** and Tb**1** revealed that both chelates crystallized in the $P\bar{1}$ space group (Table 1). The two chelates are isostructural and have 2 chelate molecules and 9 waters of crystallization in the unit cell. The PCTMB ligand occupies 7 of the 8 coordination sites of each metal ion with water excluded from the inner coordination sphere by a fourth coordinating phosphonate monoester. The source of this eighth ligand is the neighboring chelate molecule of the unit cell in much the same way as is observed for the analogous cyclen-based systems **2** and **3**[17,18] wherein the metal ions of Eu**2** and Tb**3** are sandwiched between 4 nitrogen and 4 oxygen donor atoms (Figure 1). Although superficially this appears similar to many macrocyclic octa-coordinate Ln^{3+} chelates of cyclen-based phosphonate (DOTP)[19] and phosphinate ligands, Ln**2**−**6**,[20−22] there are significant differences between the coordination environment in those chelates and the chelates of PCTMB. These differences stem primarily from the nature of the macrocyclic ring. Cyclen adopts a square conformation, defined by Dale's nomenclature[23] as [3,3,3,3], in which the nitrogen atoms are located on the sides of the ring and each ethylene bridge adopts a gauche conformation.[24−26] It has been observed that if the conformation of cyclen is distorted into a another conformation significant loss of chelate stability can sometimes result.[27] In the case of pyclen, however, the rigidity of the pyridine group dictates that one side of the macrocycle must incorporate 4 bonds and so a [3,3,3,3] conformation is impossible. Instead the macrocyclic ring adopts a [4,2,4,2] ring conformation with the nitrogen atoms located in the center of each side (Figure 2). The structure of the pyclen ring in Eu**1** (Figure 1) closely resembles that reported previously for the macrocycle alone.[28]

The incorporation of the pyridyl group into the macrocycle also has one further consequence for the chirality of the macrocyclic ring. Cyclen may adopt one of two conformations, each of which is chiral; either ($\delta\delta\delta\delta$) or ($\lambda\lambda\lambda\lambda$) conformation may be adopted according to the helicity of its ethylene bridges. Each ethylene bridge in cyclen adopts the same helicity as the others within the cyclen ring. These two conformations of cyclen may interconvert through a ring flipping motion. In contrast, the conformation of each N−C−C−N bridge in pyclen alternates around the ring, such that pyclen adopts a ($\delta\lambda\delta\lambda$) conformation. Because ($\delta\lambda\delta\lambda$) pyclen is the mirror image of ($\lambda\delta\lambda\delta$) pylcen (Figure 2), pyclen is achiral. This means that the chelates of pyclen have one fewer elements of chirality than their related cyclen-based chelates. This is significant because pyclen, once it has become part of a chelate, is unable to flip its conformation, as cyclen can, owing to the presence of the fused pyridyl ring. This means that despite being structurally rigid in a chelate, pyclen, unlike rigid cyclen derivatives,[29−31] adopts one major low energy conformation.

It is informative to compare the structures of EuPCTMB and TbPCTMB with those of the cyclen-based chelates structures Eu**2** and Tb**3**; some selected geometrical parameters of these chelates are presented in Table 2. Comparing these structures it can be seen that the two ethylene bridges of pyclen adopt gauche conformations, comparable with the cyclen derivatives. On the opposite side of the ring however, pyclen is much more strained, a consequence of including pyridine in the system. Because of the planar arrangement of the pyridine ring and its substituents in the 2- and 6- positions, the N−C−C−N torsion angles on this side of the macrocycle are approximately half that of a gauche conformation. The result is that the nitrogen atoms in the 4- and 10- positions are oriented below the level of those in the 1- and 7- positions. In contrast to cyclen, the nitrogen atoms of pyclen are not coplanar, lying about 0.4 Å above or below the mean plane (Table 2). Not surprisingly the nitrogen of the pyridine ring (N-1) lies furthest from this plane. This in turn distorts the donor oxygen atom plane of EuPCTMB and TbPCTMB by a similar amount. As a consequence, the chelates of PCTMB are unable to assume the twisted square antiprismatic (TSAP) coordination geometry adopted by the chelates of Eu**2** and Tb**3**. Instead the EuPCTMB and TbPCTMB are found to adopt a twisted snub dispheniod (TSD) coordination geometry (Figure 3). In so doing, the chelates of PCTMB are able to maintain metal-donor atom bond distances comparable to those observed in the chelates Eu**2** and Tb**3**.

Although the coordination geometry of EuPCTMB and TbPCTMB are different from those of the cyclen

(17) Senanayake, K.; Thompson, A. L.; Howard, J. A. K.; Botta, M.; Parker, D. *Dalton Trans.* **2006**, *45*, 5423–5428.
(18) Rohovec, J.; Vojtisek, P.; Hermann, P.; Ludvik, J.; Lukes, I. *Dalton Trans.* **2000**, *2*, 141–148.
(19) Avecilla, F.; Peters, J. A.; Geraldes, C. F. G. C. *Eur. J. Inorg. Chem.* **2003**, *23*, 4179–4186.
(20) Aime, S.; Batsanov, A. S.; Botta, M.; Howard, J. A. K.; Parker, D.; Senanayake, K.; Williams, G. *Inorg. Chem.* **1994**, *33*(21), 4696–4706.
(21) Aime, S.; Batsanov, A. S.; Botta, M.; Dickins, R. S.; Faulkner, S.; Foster, C. E.; Harrison, A.; Howard, J. A. K.; Moloney, J. M.; Norman, T. J.; Parker, D.; Royle, L.; Williams, J. A. G. *J. Chem. Soc., Dalton Trans.* **1997**, *19*, 3623–3636.
(22) Rohovec, J.; Vojtisek, P.; Hermann, P.; Mosinger, J.; Zak, Z.; Lukes, I. *J. Chem. Soc., Dalton Trans.* **1999**, *20*, 3585–3592.
(23) Dale, J. *Topical Stereochem.* **1976**, *9*, 199–270.
(24) Desreux, J. F. *Inorg. Chem.* **1980**, *19*(5), 1319–1324.
(25) Hoeft, S.; Roth, K. *Chem. Ber.* **1993**, *126*(4), 869–873.
(26) Meyer, M.; Dahaoui-Gindrey, V.; Lecomte, C.; Guilard, R. *Coord. Chem. Rev.* **1998**, 178–180, (Pt. 2), 1313−1405.
(27) Edlin, C. D.; Faulkner, S.; Parker, D.; Wilkinson, M. P.; Woods, M.; Lin, J.; Lasri, E.; Neth, L.; Port, M. *New J. Chem.* **1998**, *22*(12), 1359–1364.
(28) Kim, W. D.; Hrncir, D. C.; Kiefer, G. E.; Sherry, A. D. *Inorg. Chem.* **1995**, *34*(8), 2225–2232.
(29) Di Bari, L.; Pescitelli, G.; Sherry, A. D.; Woods, M. *Inorg. Chem.* **2005**, *44*(23), 8391–8398.
(30) Woods, M.; Botta, M.; Avedano, S.; Wang, J.; Sherry, A. D. *Dalton Trans.* **2005**, *24*, 3829–3837.
(31) Woods, M.; Kovacs, Z.; Kiraly, R.; Brüker, E.; Zhang, S.; Sherry, A. D. *Inorg. Chem.* **2004**, *43*(9), 2845–2851.

Table 1. Summary of Crystallographic Data for EuPCTMB and TbPCTMB

	$[EuPCTMB]_2 \cdot 9.25H_2O$	$[TbPCTMB]_2 \cdot 9.25H_2O$
empirical formula	$C_{52}\ H_{114.50}\ N_8\ O_{27.25}\ P_6\ Eu_2$	$C_{52}\ H_{114.50}\ N_8\ O_{27.25}\ P_6\ Tb_2$
molecular weight	1777.76	1791.68
temperature	383(2) K	1791.68
wavelength (Å)	0.71073	0.71069
crystal system	triclinic	triclinic
space group	$P\bar{1}$	$P\bar{1}$
a/Å	14.393(6)	14.341(6)
b/Å	16.604(7)	16.552(7)
c/Å	18.721(8)	18.666(8)
α/deg	63.924(5)	63.701(5)
β/deg	71.843(5)	71.826(5)
γ/deg	75.328(5)	75.390(5)
volume (Å^3)	3783(3)	3740(3)
Z	2	2
density (calculated)	1.561 Mg/m^3	1.591 Mg/m3
absorption coefficient (mm^{-1})	1.849	2.084
F(000)	1833	1841
crystal size (mm^3)	0.28 × 0.08 × 0.03	0.60 × 0.28 × 0.10
θ range for data collection	1.38 to 25.00°	1.91 to 25.00°
reflections collected	47807	52330
independent reflections	13185 [R(int) = 0.0467]	13015 [R(int) = 0.0561]
completeness to θ = 25.00°	98.9%	98.8%
absorption correction	semiempirical from equivalents	semiempirical from equivalents
max. and min transmission	0.9466 and 0.6255	0.8187 and 0.3678
refinement method	full-matrix least-squares on F^2	full-matrix least-squares on F^2
data/restraints/parameters	13185/1153/991	13015/1576/1070
goodness-of-fit on F^2	1.010	1.010
final R indices [$I > 2\sigma(I)$]	R1 = 0.0344, wR2 = 0.0864	R1 = 0.0629, wR2 = 0.1002
largest diff. peak and hole (e Å^{-3})	1.787 and −0.985	1.074 and −0.623

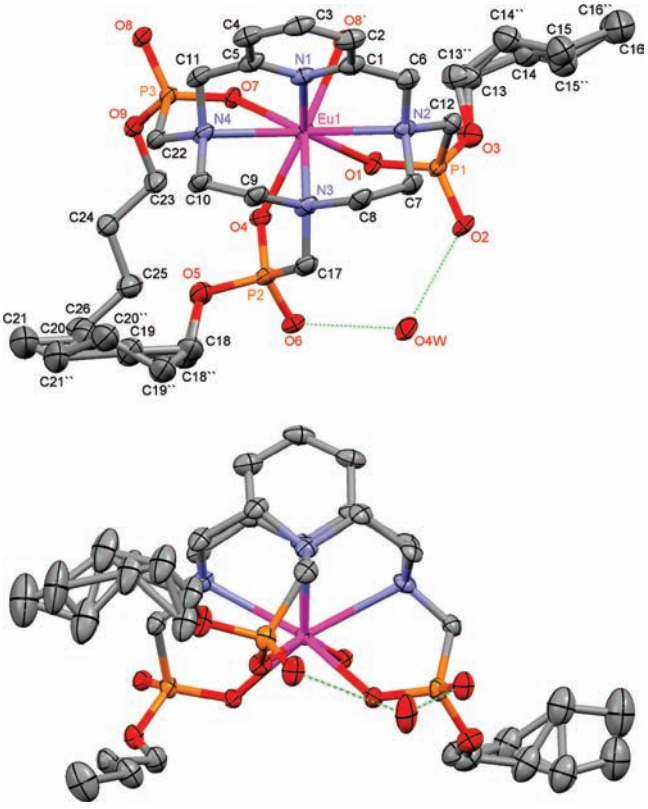

Figure 1. ORTEP rendering of the crystal structure of EuPCTMB (50% ellipsoids, dimer partner omitted) viewed from the top (above) and the side (below). Hydrogen atoms and all but the closest water molecule of crystallization have been omitted for clarity. The hydrogen bonding interaction between the closest outer sphere water molecule and two phosphonate monoesters are shown by dotted green lines. Considerable disorder may be observed in the butyl chains.

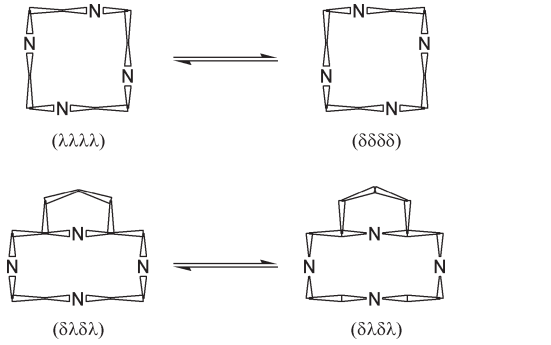

Figure 2. Conformations of cyclen (top) and pyclen (bottom) according to Dale's nomenclature.

based phosphinate and phosphonate derivatives **2**−**6** the phosphonate groups remain successful at excluding water from the inner coordination sphere. Lukeš and co-workers[32] have suggested that a critical parameter in achieving this goal is the O−M−O bond angle, β (Table 3). If this angle becomes tighter than 136° then the vacant coordination site on the metal ion becomes too sterically encumbered to accommodate a water molecule. The parameters collected in Table 3 seem to confirm this observation with angles (β) significantly smaller than 136° observed for all q = 0 chelates; a category that includes all the phosphonate and phosphinate derivatives. Indeed the narrowest O−M−O angles (β) of all are observed in the cases of EuPCTMB and TbPCTMB and arise from the different coordination geometry observed in these chelates. Although the LnPCTMB chelates have the smallest β angles, of all the chelates

(32) Lukes, I.; Kotek, J.; Vojtisek, P.; Hermann, P. *Coord. Chem. Rev.* **2001**, *216*−*217*, 287–312.

Table 2. Selected Bond Lengths [Å], Bond Angles [deg], and Distances [Å] from the Crystal Structures of EuPCTMB and TbPCTMB[a]

parameter	EuPCTMB	Eu**2**	parameter	TbPCTMB	Tb**3**
N(1)−Eu(1)	2.528	2.577	N(1)−Tb(1)	2.527	2.641
N(2)−Eu(1)	2.648	2.678	N(2)−Tb(1)	2.614	2.656
N(3)−Eu(1)	2.685	2.640	N(3)−Tb(1)	2.630	2.630
N(4)−Eu(1)	2.669	2.659	N(4)−Tb(1)	2.605	2.678
O(1)−Eu(1)	2.282	2.315	O(1)−Tb(1)	2.325	2.328
O(4)−Eu(1)	2.345	2.380	O(4)−Tb(1)	2.316	2.292
O(7)−Eu(1)	2.341	2.328	O(7)−Tb(1)	2.271	2.319
O(8′)−Eu(1)	2.272	2.310	O(2′)−Tb(1)	2.344	2.246
N(1)−N_4-plane	+0.494		N(1)−N_4-plane	+0.512	
N(2)−N_4-plane	−0.430		N(2)−N_4-plane	−0.438	
N(3)−N_4-plane	+0.365		N(3)−N_4-plane	+0.363	
N(4)−N_4-plane	−0.429		N(4)−N_4-plane	−0.437	
O(1)−O_4-plane	+0.411		O(1)−O_4-plane	+0.444	
O(4)−O_4-plane	−0.431		O(4)−O_4-plane	−0.427	
O(7)−O_4-plane	+0.432		O(7)−O_4-plane	+0.400	
O(8′)−O_4-plane	−0.412		O(2′)−O_4-plane	−0.417	
N(1)−C−C−N(2)	−31.1	59.2	N(1)−C−C−N(2)	−39.9	60.5
N(2)−C−C−N(3)	+60.03	57.5	N(2)−C−C−N(3)	+54.1	60.9
N(3)−C−C−N(4)	−53.85	57.8	N(3)−C−C−N(4)	−62.9	56.1
N(4)−C−C−N(1)	+40.47	59.2	N(4)−C−C−N(1)	+29.0	62.6

[a] For comparative purposes the values for Eu**2** and Tb**3** have also been included from refs 17 and 18, respectively. The N_4- and O_4-planes are the mean planes of the four nitrogen and four oxygen atoms, respectively.

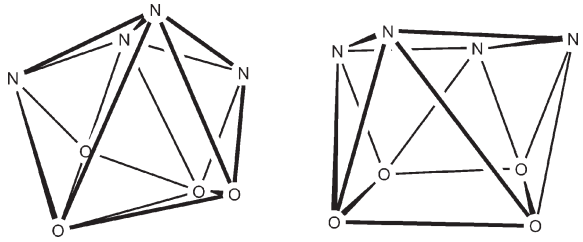

Figure 3. Coordination geometry of a twisted snub dispheniod (TSD) adopted by the pyclen derivatives EuPCTMB and TbPCTMB (left) and the twisted square antiprism (TSAP) commonly adopted by methylene phosphonate and phosphinate derivatives of cyclen (right).

collected in Table 3 they also have the largest β' angles, notably the O−M−O angles are much larger than the critical 136° required by Lukes et al. for water coordination, and yet these chelates remain $q = 0$. These large differences in O−M−O angles are partly the result of the [4,2,4,2] ring conformation observed in these chelates that also results in a very narrow N−M−N bite angle, which, it should be noted, is not entirely symmetrical. The presence of the pyridine ring results in one side of the macrocycle being brought closer to the metal ion, with the other, more flexible, side bowed out slightly. This is in sharp contrast to the near perfect symmetry observed in the structure of GdDOTP.[19]

In chelates of DOTA and DOTAM, both of which possess one bound water molecule ($q = 1$), the Ln^{3+} ion lies much closer to the 4 oxygen donor atoms than it does to the 4 nitrogen donors. For these chelates the metal ion is typically found to lie approximately 7/10 of the distance (d/c, Table 3) to the mean oxygen atom plane, irrespective of which coordination geometry (SAP or TSAP) is observed.[33] In contrast the d/c ratios for the $q = 0$ cyclen-based phosphonate and phosphinate chelates (Table 3) are much smaller (typically ≈ 0.62), indicating that the Ln^{3+} ion lies significantly closer to the mean nitrogen plane. Significantly, the d/c ratios of EuPCTMB and TbPCTMB are in line with those observed for these cyclen-based phosphonate and phosphinate systems. Although the distance between the mean nitrogen and oxygen atom planes is about 0.15 Å greater in the phosphonate and phosphinate systems compared with the acetate and amide systems, the metal also lies closer to the nitrogen plane in absolute terms, by about 0.1 Å. The crystal structures of the Ln^{3+} chelates of ligands **3** and **4** and their d/c ratios provides some insight into the relationship between the position of the Ln^{3+} ion and the hydration state (q value) of the chelate. The crystal structures of Ln**3** chelates across the lanthanide series reveal that the d/c ratio falls across the series, reaching a minimum of about 0.61 at europium and remaining more or less constant thereafter. Thus, the chelates of the smaller heavy lanthanides Eu**3**, Tb**3**, Er**3**, Yb**3**, Eu**4**, and Y**4**, all of which are $q = 0$, have small d/c ratios, between 0.61 and 0.63.[18] Nd**3** has slightly larger d/c ratio, 0.65, but a small O−M−O bond angle, 129°, and is also $q = 0$.[18] However, chelates of larger Ln^{3+} ions La**4**, La**3**, and Ce**3** are $q = 1$ and have d/c ratios comparable to those of DOTA and DOTAM chelates, $d/c = 0.68-0.70$.[18,21] The smaller of the two O−M−O bond angles (β) in the chelates of La**3** and Ce**3** are 135°,[18] a shade narrower than the cutoff proposed by Lukeš and co-workers,[32] and yet a water molecule is still able to coordinate with the metal center. The crystal structure of Pr**3**, presented subsequently,[34] provides reason for pause at this point; it is presented as a $q = 1$ chelate and yet has $\beta = 129.7°$ and $\beta' = 136.4°$ and a relatively small d/c ratio of 0.65. It is not until one considers that the reported water bond distance, 2.820 Å, is longer than is normally considered a bonding interaction that we can really understand this chelate. Pr**3** is, in reality, probably $q = 0$ but is able to maintain an interaction with a water molecule as a result of its d/c ratio. This evidence suggests that when the Ln^{3+} ion in

(33) Vipond, J.; Woods, M.; Zhao, P.; Tircso, G.; Ren, J. M.; Bott, S. G.; Ogrin, D.; Kiefer, G. E.; Kovacs, Z.; Sherry, A. D. *Inorg. Chem.* **2007**, *46*(7), 2584–2595.

(34) Klimentova, J.; Vojtisek, P. *J. Mol. Struct.* **2007**, *826*(2−3), 82–88.

Table 3. Selected Geometrical Parameters of the Structures of EuPCTMB, TbPCTMB, and Some Related Cyclen Derived Chelates[a]

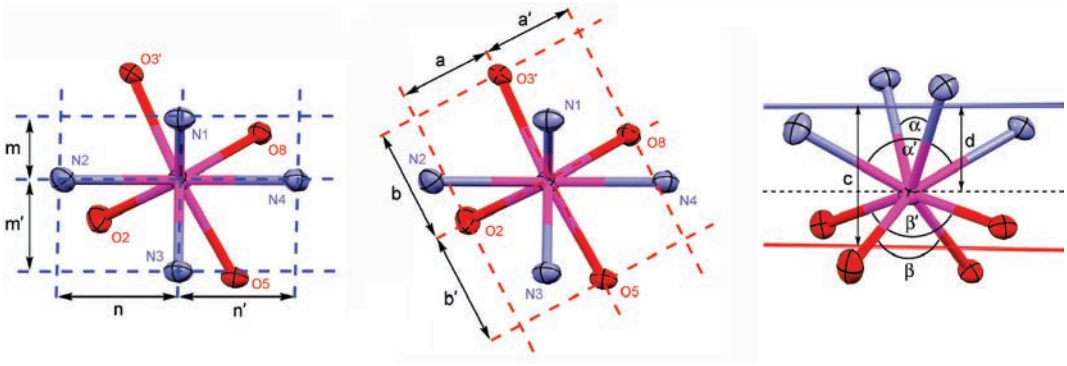

Chelate	EuPCTMB	TbPCTMB	Eu**2**[b]	Eu**3**[c]	GdDOTP[d]	CeDOTA[e]	PrDOTAM[f]
Coordination geometry	TSD	TSD	TSAP	TSAP	TSAP	TSAP	TSAP
θ [deg]			30.3	29.6	23.6	24.4	22.9
q	0	0	0	0	0	1	1
α [deg]	70.4	72.1	101.0	103.0	104.0	98.9	100.5
α′ [deg]	123.8	125.1	106.3	103.8	104.0	100.1	101.5
β [deg]	102.8	100.4	127.3	123.2	126.5	143.5	140.9
β' [deg]	150.3	148.4	130.6	133.5	126.5	145.0	143.3
c [Å]	2.703	2.686	2.633	2.670	2.685	2.520	2.528
d [Å]	1.682	1.638	1.629	1.659	1.643	1.765	1.735
d/c	0.62	0.61	0.62	0.62	0.61	0.70	0.69
a [Å]	2.341	1.968	2.123	2.060	2.066		
a' [Å]	1.940	1.504	2.071	2.229	2.066		
b [Å]	2.307	2.258	2.069	2.032	2.066		
b' [Å]	2.252	2.224	2.147	2.342	2.066		
m [Å]	1.284	1.204	1.961	2.079	2.101		
m' [Å]	1.737	1.817	2.064	2.082	2.101		
n [Å]	2.669	2.316	2.151	2.126	2.101		
n' [Å]	2.341	2.316	2.120	2.118	2.101		
N−C−X−O [deg] (max)[g]	36.6	39.4	25.6	32.3	33.8	31.7	29.4
N−C−X−O [deg] (min)[g]	20.3	19.0	17.2	19.1	33.8	23.2	16.5

[a] Atom labels are given according to the numbering scheme used for the structure of EuPCTMB. [b] Data from ref 17. [c] Data from ref 18. [d] Data from ref 19. [e] Data from ref 35; DOTA is 1,4,7,10-tetraazacyclododecane tetraacetic acid. [f] Data from ref 36; DOTAM is 14,7,10-tetraazacyclododecane tetraacetamide. [g] X = P, except for DOTA and DOTAM where X = C.

aza-crown based chelates such as these is octa-coordinate and a water molecule is absent from its coordination sphere, the Ln^{3+} ion moves toward the amines of the macrocycle in search of increased electron density. The question as to which comes first, movement of the Ln^{3+} ion or departure of the water molecule, is something of a "chicken and the egg problem". However, it seems clear that this has implications for understanding dissociative water exchange processes during which it now seems likely that the position of the Ln^{3+} ion fluctuates according to the hydration state of the chelate. It also implies that the d/c ratio may provide a better delineation between chelates that can be hydrated ($q = 1$) and those that cannot ($q = 0$) given that the O−M−O angle may vary significantly, even within the same chelate. It seems that one may conclude from this that a d/c ratio much smaller than 0.68 will result in water being excluded from the inner coordination sphere, but that until this ratio is smaller than 0.65, non-bonding interactions between metal and water are still possible.

Owing to the absence of chirality in the pyclen ring, the chirality of an LnPCTMB chelate is determined by the orientation of the pendant arms (Δ or Λ) and the configuration at phosphorus (*R*- or *S*-). The prochiral phosphorus atom of the ligand becomes chiral upon coordination with the metal ion, so either configuration may be a result from the synthesis of the chelate. Studies into the solution and solid state structures of Ln**4** and Ln**5** chelates have shown an interdependence of the orientation of the pendant arms and the configuration at phosphorus.[20,37] A single C_4-symmetric coordination isomer predominates in solution for Ln**4** and Ln**5** chelates, while crystal structure data reveals that a Λ orientation of the pendant arms is associated with an *R*- configuration at phosphorus and a Δ orientation with an *S*-configuration at phosphorus.[20,21] This observation is reminiscent of that observed in α-substituted acetate derivatives of cyclen.[29,38−40] In sharp contrast, these two elements of

(35) Benetollo, F.; Bombieri, G.; Calabi, L.; Aime, S.; Botta, M. *Inorg. Chem.* **2003**, *42*(1), 148–157.
(36) Bombieri, G.; Marchini, N.; Clattini, S.; Mortillaro, A.; Aime, S. *Inorg. Chim. Acta* **2006**, *359*(10), 3405–3411.
(37) Aime, S.; Botta, M.; Dickins, R. S.; Maupin, C. L.; Parker, D.; Riehl, J. P.; Williams, J. A. G. *J. Chem. Soc., Dalton Trans.* **1998**, *6*, 881–892.
(38) Howard, J. A. K.; Kenwright, A. M.; Moloney, J. M.; Parker, D.; Woods, M.; Port, M.; Navet, M.; Rousseau, O. *Chem. Commun.* **1998**, *13*, 1381–1382.
(39) Woods, M.; Aime, S.; Botta, M.; Howard, J. A. K.; Moloney, J. M.; Navet, M.; Parker, D.; Port, M.; Rousseaux, O. *J. Am. Chem. Soc.* **2000**, *122*(40), 9781–9792.
(40) Di Bari, L.; Pintacuda, G.; Salvadori, P. *Eur. J. Inorg. Chem.* **2000**, *1*, 75–82.

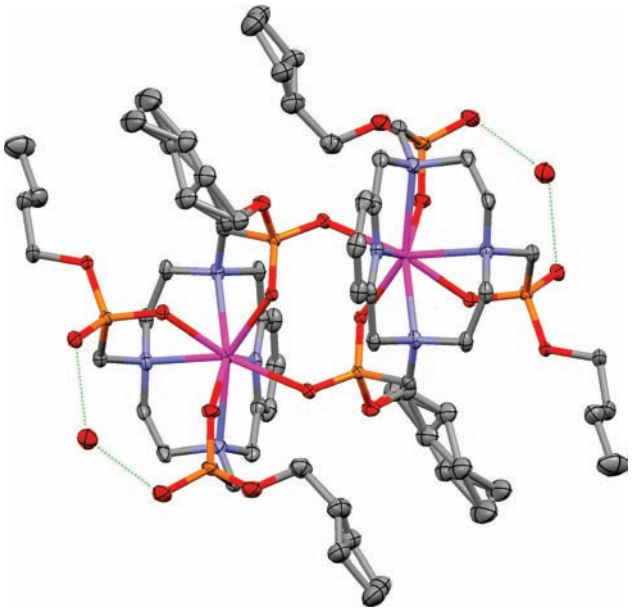

Figure 4. ORTEP rendering of the crystal structure of Tb**1** (50% ellipsoids) showing the dimeric nature of the chelate. Hydrogens have been omitted for clarity.

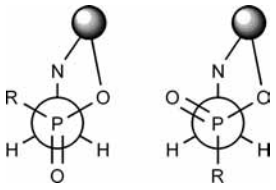

Figure 5. Conformation of the pendant arms in the Ln^{3+} chelates of PCTMB, **2**, and **3**, with the substituent gauche to the coordinating amine (left) and anti to the coordinating amine (right).

chirality do not exhibit any such interdependence in the Ln**6** chelates, despite the apparent structural similarity of the ligand systems.[22] Multiple isomers of Ln**6** chelates are observed in solution and, at least in the crystal, the pendant arms bind cooperatively (i.e., with the same helicity) even though the configuration at phosphorus alternates *RSRS*- around the ring.

The structures of LnPCTMB, Ln**2**, and Ln**3** chelates in the crystal share some common features (Figure 4 and Supporting Information, Figures S1 and S2). Each chelate is present in a dimer. The dimer is associated by two bridges in which one phosphonate of each chelate coordinates to both Ln^{3+} ions of the dimer. For each of these chelates the dimer is made up of two chelate molecules that are enantiomers of one another. The pendant arms bind cooperatively, with one molecule of the dimer exhibiting a Δ orientation and its partner a Λ orientation. However, when it comes to the configuration at phosphorus, these chelates resemble Ln**6** chelates more than either the Ln**4** or the Ln**5** chelates. Clearly, the configuration at phosphorus is strongly influenced by the nature of the phosphorus R-substituent. In the structures of LnPCTMB, Ln**2**, and Ln**4** the preferred conformation of the pendant arm is with the R-substituent of phosphorus in a gauche position with respect to the nitrogen of the macrocycle (Figure 5). However, in the case of Ln**3** chelates the R-substituent exhibits a preference for a position anti- to the nitrogen of the macrocycle, with only the middle arm adopting the gauche conformation preferred in the chelates of PCTMB, **2**, and **4**.

In both LnPCTMB and Ln**3** chelates phosphorus adopts *RSR*-/*SRS*- configurations going around the macrocyclic ring. In contrast, the configuration at phosphorus in Ln**2** chelates is *RRS*-/*SSR*-, this despite the interdependence with pendant arm orientation observed in the analogous tetra-phosphinate chelates Ln**4** and Ln**5**. Notably, it is the pendant arm that bridges the two chelate molecules that has the inverted configuration at phosphorus, and it is only through this inversion of configuration that the pendant arm is able to make a second oxygen donor atom available for coordination in the dimeric structure (Supporting Information, Figures S1). It appears that in the case of Ln**2**, the energy penalty incurred by placing the phosphorus R-substituent into an *anti*- position is more than compensated for by the drop in energy, and increase in enthalpy, associated with dimerization of the chelate.

It is less clear why the central pendant arm of LnPCTMB and Ln**3** chelates should adopt an *anti*- conformation. One explanation may lie in a phenomenon exhibited by both chelates and clearly visible by inspection of Figure 2; by inverting the configuration of the middle pendant arm these chelates are able to bind a second sphere water molecule in a pincer action. Hydrogen bonded by both non-bridging phosphonates, this water molecule lies closest to the metal ion, 5.574 Å from the Eu^{3+} ion and 5.476 Å from Tb^{3+}, and may have a residence lifetime on the chelate long enough to have significance in relaxometric studies of the Gd^{3+} chelate. Notably this pincer binding action used to hold water molecule is absent from the structures of Ln**2** chelates. As a result the 4 s sphere water molecules of Ln**2** chelates are hydrogen bonded to just one phosphinate each and lie further from the metal ion, over 6.5 Å away.

Solution State Studies. The dimeric forms of Ln**2** and Ln**3** chelates that are observed in the crystal structure have also been shown to persist in the solution state.[17,18] The presence of dimeric structures in solution may be beneficial, as in the case of luminescent probes, or detrimental, as in the case of an MRI contrast agent. For these reasons it is important to understand the behavior of the dimeric structure of PCTMB chelates in solution. LnPCTMB chelates are minimally soluble in water at room temperature. However, upon heating to reflux it is possible to obtain a chelate solution that is 1−2 mM, which persists after cooling. Solutions of EuPCTMB and TbPCTMB are brilliantly luminescent when irradiated with common UV sources which provide a convenient tool for probing their sensitized photophysical properties.

Relaxometric Studies. Rapidly exchanging water molecules in the inner-coordination sphere of a gadolinium ion contribute significantly to its overall relaxivity. Clearly then a chelate that excludes all water molecules from the inner-coordination sphere is likely to be ineffective as an MRI contrast agent. Relaxivity (r_1) is the measure of how effective a contrast agent and is defined as the increase in longitudinal relaxation rate per unit concentration of contrast agent. Relaxivity is usually

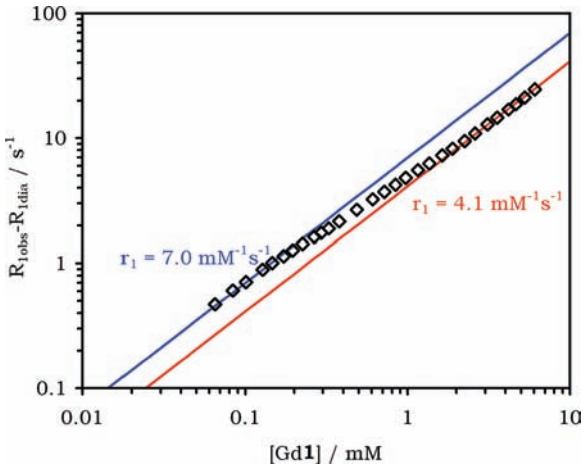

Figure 6. Dependence of the paramagnetic contribution to R_1 upon the concentration of GdPCTMB is non-linear (20 MHz, 298 K).

determined by measuring the longitudinal relaxation rate (R_1 which = $1/T_1$) of solutions of the contrast agent at different concentrations. A linear regression analysis then affords the relaxivity as the slope of the line. Accordingly, the longitudinal relaxation rates of solutions of GdPCTMB were measured over the concentration range 0.06−6.0 mM. Measurements were performed in 2:1 v/v water/methanol solution, owing to the poor solubility of the chelate in water at concentrations as high as 6.0 mM. The results, shown in Figure 6 on a logarithmic axis for greater clarity, reveal that R_1 is not linearly dependent upon the concentration. This non-linearity is most usually observed if a structural change, that alters relaxivity, occurs as a result of a change in concentration. Fitting data in the concentration ranges 0.06−0.2 mM and 2.0−6.0 mM confirms this observation. The data in each of these two concentration ranges fits well to a straight line (Figure 6). Data fitting in the high concentration range affords a value of r_1 = 4.1 mM^{-1} s^{-1}. In contrast, the low concentration range affords a value of r_1 = 7.0 mM^{-1} s^{-1}.

These observations are consistent with dissociation of the dimeric structure of GdPCTMB, observed in the crystal structures of EuPCTMB and TbPCTMB, as the concentration of the chelate is decreased. The relaxivity of GdPCTMB obtained at higher concentrations (r_1 = 4.1 mM^{-1} s^{-1} at >2.0 mM) is significantly higher than that observed for Gd**2** (r_1 = 1.9 mM^{-1} s^{-1} at 0.1 mM) which was shown to exist solely as a dimer across the entire concentration range studied.[17] Parker and co-workers described Gd**2** as an entirely outer-sphere chelate owing to this dimerization phenomenon in solution.[17] It seems reasonable to believe that at higher concentration, above 2.0 mM, GdPCTMB exists solely in a dimeric form in solution; the enhanced relaxivity of this chelate can then be ascribed to the effect of water molecules in the second hydration sphere. As described earlier LnPCTMB chelates appear to bind water molecules in the second-hydration sphere using two phopshonate monoesters in a pincer action; this not only decreases the distance of closest approach of molecules in the second hydration sphere but may reasonably be expected to increase their residence lifetime on the chelate. It is now well established that a long-lived second-hydration sphere in Gd^{3+} complexes can lead to substantial relaxivities,[41] even in the absence of an inner-hydration sphere; GdDOTP is just one example of this.[42] It then appears that as the concentration of GdPCTMB decreases the chelate begins to dissociate, permitting water into the inner coordination sphere. By allowing water into the inner coordination sphere, the relaxivity of the chelate is increased to 7.0 mM^{-1} s^{-1}. It seems apparent that LnPCTMB chelates, unlike the analogous Ln**2** and Ln**3** chelates, do not persist as doubly bridged dimers in solution over a wide concentration range. Rather, the extent of dimerization in LnPCTMB chelates is highly concentration dependent, a conclusion supported by the results of luminescent studies on EuPCTMB.

Luminescence Studies. The luminescent properties of Eu^{3+} can provide valuable insight into the speciation of its chelates in solution. In addition to allowing the hydration state (q value) to be determined using Horrocks' method,[43,44] later modified by Parker and co-workers,[45] the $^5D_0 \rightarrow {}^7F_0$ transition of the Eu^{3+} emission spectrum provides a single line for each Eu^{3+} species present in solution, the result of the non-degeneracy of both the $^5D_0$ and the $^7F_0$ states. Providing that the energy of this transition is different for each species in solution, it is possible to examine each species individually by following this transition. Examining this transition has been used with considerable success in examining hydration equilibria in Eu^{3+} chelates.[46] However, to examine the $^5D_0 \rightarrow {}^7F_0$ transition it is necessary to acquire the emission spectrum with high spectral resolution, 0.1 nm or better. The high resolution emission spectrum of EuPCTMB in the crystalline phase (Figure 7, bottom) is characteristic of a single Eu^{3+} coordination environment. A single $^5D_0 \rightarrow {}^7F_0$ transition is observed and the 3 transitions expected for the $^5D_0 \rightarrow {}^7F_1$ transition of a chelate of this type[39] are visible and clearly spaced. Dissolution in water at 0.4 mM significantly changes the nature of the emission spectrum (Figure 7 top); most clearly the two lines observed for the $^5D_0 \rightarrow {}^7F_0$ transition indicate that two Eu^{3+} coordination environments are now present. The line at 580.4 nm corresponds closely to the single line observed for the dimer in the crystalline phase at 580.2 nm. The new line, observed at 579.8 nm, may be ascribed to the presence of a hydrated form of the Eu^{3+} chelate in solution.

Hydration of a Ln^{3+} center in this new species was confirmed by determining the q values using an adaptation of Horrocks' method.[45] Owing to the poor solubility of the chelates in aqueous solution, the hydration state determination was performed on the more emissive Tb^{3+} chelate. Following excitation at 280 nm and monitoring

(41) Botta, M. *Eur. J. Inorg. Chem.* **2000**, *3*, 399–407.
(42) Geraldes, C. F. G. C.; Sherry, A. D.; Lazar, I.; Miseta, A.; Bogner, P.; Berenyi, E.; Sumegi, B.; Kiefer, G. E.; McMillan, K..; et al. *Magn. Reson. Med.* **1993**, *30*(6), 696–703.
(43) Horrocks, W. D.; Sudnick, D. R. *J. Am. Chem. Soc.* **1979**, *101*(2), 334–340.
(44) Horrocks, W. D.; Sudnick, D. R. *Acc. Chem. Res.* **1981**, *14*(12), 384–392.
(45) Beeby, A.; Clarkson, I. M.; Dickins, R. S.; Faulkner, S.; Parker, D.; Royle, L.; de Sousa, A. S.; Williams, J. A. G.; Woods, M. *J. Chem. Soc., Perkin Trans. 2* **1999**, *3*, 493–504.
(46) Wu, L. W.; Horrocks, D. J. *Anal. Chem.* **1996**, *68*, 394–401.

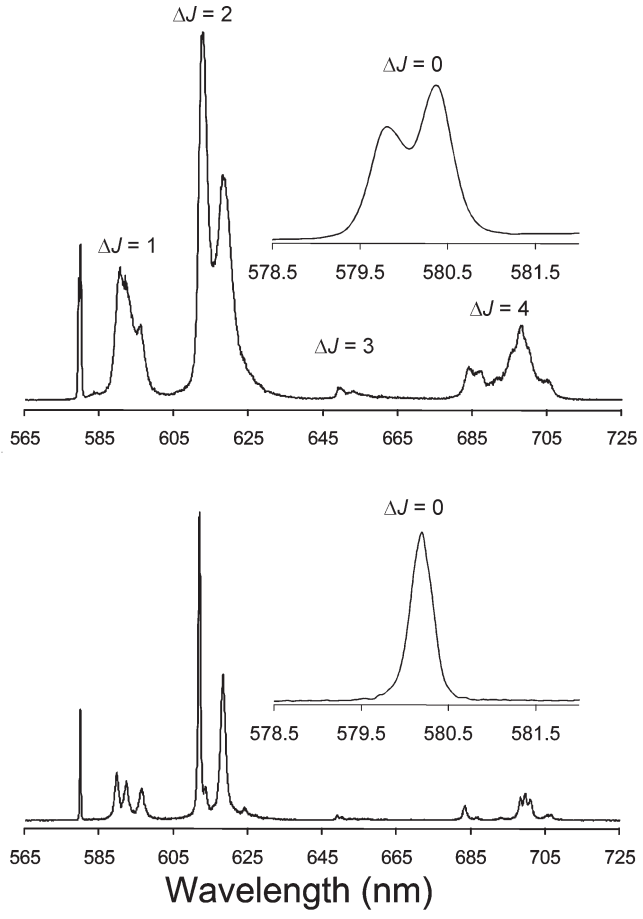

Figure 7. Emission spectra of EuPCTMB (λ_{ex} = 280 nm) in solution at 0.43 mM (top) and in the crystal (bottom). The inset in each spectrum shows the non-degenerate $^5D_0 \rightarrow {}^7F_0$ transition, highlighting the number of species present (λ_{ex} = 280 nm).

Table 4. Hydration State Determination of TbPCTMB in Aqueous Solution at 0.15 mM Using an Adaptation[45] of Horrocks' Method[43,44] [a]

τ_{H_2O} (ms)	τ_{D_2O} (ms)	q
2.50 ± 0.25	3.11 ± 0.31	0.09 ± 0.01
1.43 ± 0.14	2.32 ± 0.23	1.04 ± 0.10

[a] Data were collected using λ_{ex} = 280 nm, λ_{em} = 545 nm, and fitted to a double exponential model of decay to provide the lifetime for each Tb^{3+} coordination environment.

emission at 545 nm the decay of Tb^{3+}-based luminescence from a 0.15 mM solution of TbPCTMB was monitored. Double exponential decay of the Tb^{3+} excited state was observed for TbPCTMB. For chelates with a single hydration state, a single exponential decay is expected; a double exponential decay is indicative of the presence of two different Tb^{3+} hydration states. Fitting the luminescent decay curve to a double exponential model (Table 4 and Supporting Information, Figures S3) revealed that two species were present, with the more prevalent species $q = 0$ and the less prevalent $q = 1$.

The simplest explanation for these results is that dissolution in water leads to dissociation of the dimeric structure observed in the crystal and that in solution a mixture of discrete monomer and dimer are present. However, it is important to keep in mind that the emission spectrum of Eu^{3+} affords information limited to the immediate coordination environment of the Eu^{3+} ion. In the event that a bridging phosphonate were replaced by a water molecule, this change would most likely be reflected by a change in the emission spectrum of Eu^{3+} to a change in the spectrum and in particular the $\Delta J = 0$ transition. A simple monomer/dimer equilibrium would be expected to be characterized by a change in the relative intensities of the two $\Delta J = 0$ transitions that was directly dependent upon the chelate concentration.

The Eu^{3+} $\Delta J = 0$ transitions in the emission spectra of EuPCTMB were examined as a function of the concentration of the chelate in solution (Figure 8). Over the concentration range 4.3×10^{-1} M to 4.3×10^{-4} M, two lines were observed for this transition. Of these, the line at 580.2 nm (ascribed to the dimeric structure, vide infra) is more intense at higher concentrations and, as the solution becomes more dilute, this line becomes relatively less intense. The relative intensity of the line at 579.8 nm (ascribed to a hydrated Eu^{3+} ion, vide infra) is found to increase as the solution becomes more dilute. However, the trend of these changes is non-linear with respect to chelate concentration which would seem to indicate that a complicated set of equilibria exist in solutions of LnPCTMB chelates. It is also worth noting that given the millisecond time scale of the $^5D_0 \rightarrow {}^7F_0$ measurements, all observable species must be exchanging at a rate slower than100 Hz.

Examination of the $^5D_0 \rightarrow {}^7F_0$ transition in Eu^{3+} chelates is unlikely to be able to distinguish between the presence of a simple monomer/doubly bridged dimer equilibrium and a more complex equilibrium that also involves a singly bridged dimer (Chart 2). This latter scenario would involve a species that had two Eu^{3+} coordination environments neither of which could be readily distinguished from a monomer/doubly bridged dimer equilibrium. To probe the extent of dimerization in aqueous solution, the Stern−Volmer quenching of EuPCTMB by NdPCTMB was assessed using a similar procedure to that reported by Morrow et al.[47] Stern−Volmer quenching constants of $K_{SV}{}^{\tau} = 1101 \pm 61$ M^{-1} and $K_{SV}{}^{\Phi} = 40780 \pm 2531$ M^{-1} were thus obtained. Given that the $K_{SV}{}^{\tau}$ is predominantly determined by dynamic, or collisional, quenching, it is to be expected that this value would remain largely constant regardless of the extent of dimerization. $K_{SV}{}^{\Phi}$ is a reflection both static and dynamic quenching, the static component of which will only be present when dimerization causes an increase in the rate of excited state deactivation. Thus, in a purely monomeric system $K_{SV}{}^{\Phi}$ should have the same value as $K_{SV}{}^{\tau}$; however, in this case the large disparity between the two values is a clear indicator of dimerization. From the extremely high $K_{SV}{}^{\Phi}$ value, we can conclude that the extent of dimerization far exceeds the levels of doubly bridged dimer that one may expect from Figure 8 and that substantial quantities of singly bridged dimer are present in aqueous solution.

This conclusion is consistent with the relaxometric results. Care should be taken not to draw parallels that

(47) Amin, S.; Voss, D. A.; Horrocks, W. D.; Morrow, J. R. *Inorg. Chem.* **1996**, *35*(26), 7466–7467.

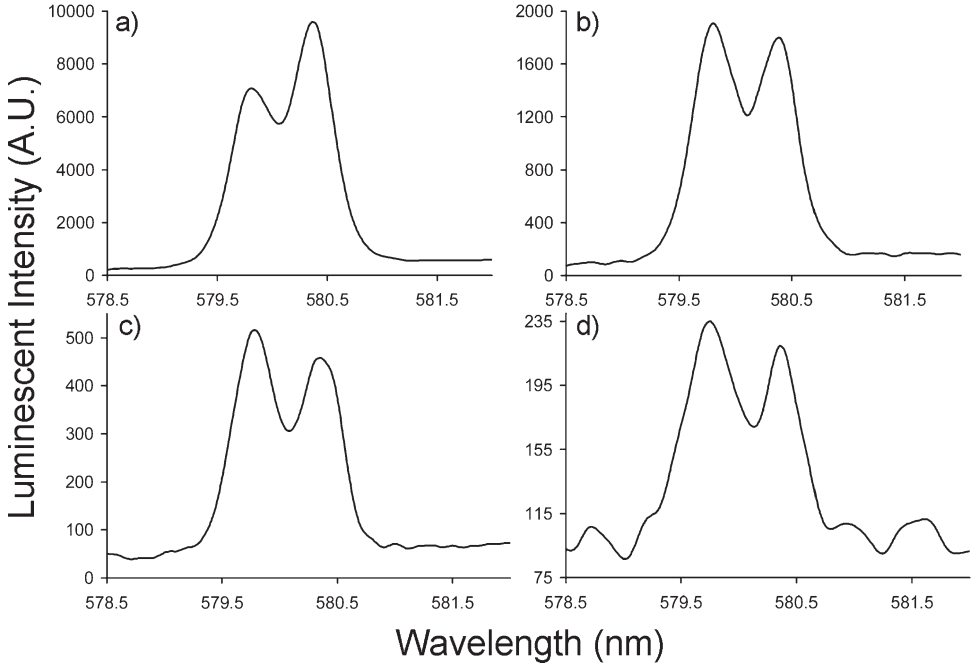

Figure 8. $^5D_0 \rightarrow {}^7F_0$ transition of the Eu^{3+} emission spectra (λ_{ex} = 280 nm) of EuPCTMB in aqueous solution at (a) 4.3×10^{-3} M; (b) 4.3×10^{-4} M; (c) 4.3×10^{-5} M; and (d) 4.3×10^{-6} M.

Chart 2. Structures of the Three Components Thought to Make up the Solution State Equilibrium in Aqueous EuPCTMB Samples

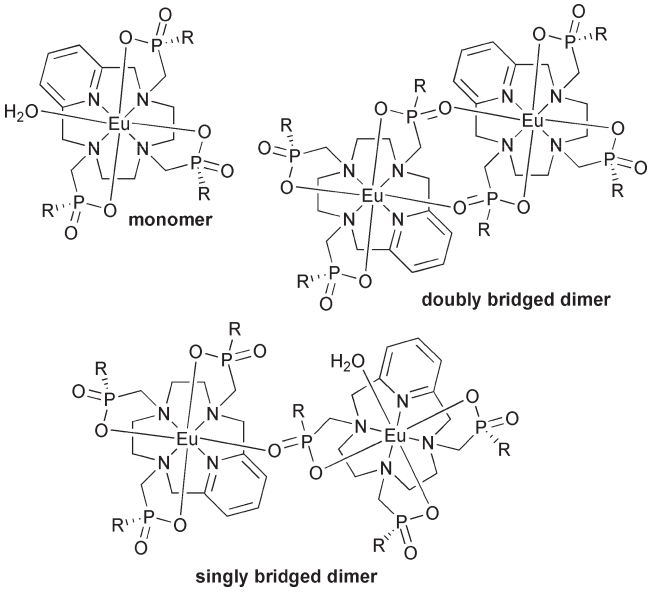

are too close between these two sets of experiments because different solvent systems were employed in each case; Senanayake et al. observed substantially different speciation of Ln**2** upon addition of methanol to an aqueous solution of the chelate.[17] Nonetheless, if a decrease in chelate concentration leads to progressively more singly bridged dimer, in which one Gd^{3+} ion is hydrated, then this would reasonably be expected to increase relaxivity. The relatively large hydrodynamic volume of this species would enhance τ_R, while allowing water access to the inner hydration sphere of one Gd^{3+} ion of the dimer would introduce an effectively large inner-sphere contribution to relaxivity. We may postulate that this is the origin of the concentration dependent relaxivity of GdPCTMB.

Conclusions

The Ln^{3+} chelates of PCTMB provide a fascinating insight into the behavior of macrocyclic Ln^{3+} chelates and in particular those of triphosphonate-based ligands. In the crystal the chelates exist as doubly bridged dimers in which all water is excluded from the inner coordination sphere of the Ln^{3+} ion. This behavior closely parallels that of related cyclen-based phosphinate systems, Ln**2** and Ln**3**. However, in solution the behavior is substantially different from the cyclen-based systems. Although Ln**2** and Ln**3** chelates are reported to exist exclusively as dimers in aqueous solution the speciation of solutions of LnPCTMB chelates is not only complex but highly concentration dependent. There can be little doubt that a certain amount of dimer dissociation occurs in solution, this gives rise to observation of a $q = 1$ species in the Tb^{3+} chelate, an additional line in the $^5D_0 \rightarrow {}^7F_0$ transition of the Eu^{3+} emission spectrum, and enhanced relaxivity of the Gd^{3+} chelate at low concentrations. The results of Stern−Volmer experiments show that in addition to a mixture of monomer and doubly bridged dimer, a substantial proportion of singly bridged dimer (Chart 2) must also be present. Ultimately, the considerable relaxivity afforded by the Gd^{3+} chelate and strong emissive properties of the Eu^{3+} and Tb^{3+} chelates of PCTMB, along with the known tumor targeting properties of these chelates,[16] affords a system of considerable interest for further study, in vivo imaging, and therapy applications.

Acknowledgment. The authors thank the National Institutes of Health (EB-04285), Portland State University and Oregon Health and Science University for financial assistance. We also thank Joseph Reibenspies

of Texas A&M University for acquiring x-ray structural data.

Supporting Information Available: Images of the crystal structure of Ln**2** and Ln**3**; fitting of the luminescent decay, and steady state spectra of TbPCTMB; Stern−Volmer plots; crystallographic data (.cif files) of the two crystal structures. This material is available free of charge via the Internet at http://pubs.acs.org. CCDC 752333 and 752334 contains the supplementary crystallographic data for this paper. These data can be obtained, free of charge, from The Cambridge Crystallographic Data Centre via www.ccdc.cam.ac.uk/data_request/cif.